Advance View
https://doi.org/10.3354/meps14424

MARINE ECOLOGY PROGRESS SERIES
Mar Ecol Prog Ser

November 9, 2023

Contribution to the Theme Section 'Small pelagic fish: new research frontiers'

Hiding in plain sight: predator avoidance behaviour of mesopelagic *Maurolicus muelleri* during foraging

Kjetil Gjeitsund Thorvaldsen*, Stefan Neuenfeldt, Patrizio Mariani, J. Rasmus Nielsen

National Institute of Aquatic Resources, Technical University of Denmark, 2800 Kongens Lyngby, Denmark

ABSTRACT: Mesopelagic fishes are ubiquitous, ecologically important and a potential protein resource. However, how mesopelagic fish use their 3D environment and facilitate encounters is fairly unknown. We tracked the swimming trajectories of juvenile *Maurolicus muelleri* and adult *M. muelleri* and *Benthosema glaciale* acoustically within 2 distinct vertical layers, measured swimming speed, and used a self-overlap model to analyse the geometry of the trajectories. Our aim was to investigate if and how the fishes were optimizing their swimming behaviour, maximizing prey encounters while minimizing predator encounters simultaneously, and how different ontogenetic stages move differently in the 2 layers. We found that some of the mesopelagic fishes were moving actively, displaying a range between ballistic and convoluted movements. Some of the fishes, especially the adults, had higher degrees of self-overlap, reducing predator encounters. Juveniles took higher risks, increasing the potential for prey encounters. Individual behaviour was highly variable and may be in response to differing ontogenetic stages, potential predator and prey surroundings, and abiotic factors such as light, water turbulence and currents. The presence of active individual spatial behaviour challenges the assumption of mass action in modelling species interactions and underlines the importance of accounting for environmental changes modifying individual-level predator–prey encounter conditions.

KEY WORDS: Mesopelagic fish · Movement ecology · Target tracking · Acoustics · Trophic interactions · Self overlap

1. INTRODUCTION

Motion is a key element in the ecology of living organisms, and it is a critical parameter that both drives evolution and population ecology (Nathan 2008). For the individual organism, motion affects interactions with prey, mates and predators (Nathan 2008, Barraquand & Murrell 2013, Martinez-Garcia et al. 2020). Motion has large effects on encounter rates, regulating encounters with prey, predators and conspecifics. This impacts on survival and reproductive success. Behaviours that increase the likelihood for survival by reducing predator encounters while optimizing foraging opportunities are selected by evolution over a range of organisms and ecological trophic levels (Nathan 2008).

Simple models have historically been applied in describing encounter rates (Holling 1959, 1966, Gerritsen & Strickler 1977, Rothschild & Osborne 1988). However, the described motion patterns have been simplified due to lack of observation methods (Nathan 2008, Martinez-Garcia et al. 2020, O'Dwyer 2020). Observing animal motion, especially in aquatic environments, has been challenging due to the lack of target-tracking methodologies. Usually these methodologies have been reserved for large-sized animal groups (Hays et al. 2016).

Improved monitoring methods for aquatic organisms, such as split-beam echosounders (Ehrenberg & Torkelson 1996, Ona 1999, Torgersen & Kaartvedt 2001, Handegard et al. 2005, Klevjer & Kaartvedt 2006, Handegard 2007, Christiansen et al. 2019,

*Corresponding author: kjgth@aqua.dtu.dk

2021), acoustic cameras (Handegard et al. 2012, Ashraf et al. 2016, Rieucau et al. 2016, Kandimalla et al. 2022) and video cameras (Edgington et al. 2006, Bianco et al. 2014, Tomaru et al. 2016, Qian & Chen 2017, Lucas et al. 2021, Burns et al. 2022, Gong et al. 2022) have created new opportunities to investigate small-sized marine organisms in their natural environments.

Mesopelagic fishes likely play an important role in controlling global carbon sequestering (Hidaka et al. 2001, Davison et al. 2013, Saba et al. 2021). They are a major potential protein source for human consumption (Alvheim et al. 2020, Grimaldo et al. 2020, Standal & Grimaldo 2020, Paoletti et al. 2021, van der Meer et al. 2023). Mesopelagic fishes are known for choosing specific ambient light levels for efficient foraging (Clark & Levy 1988, Langbehn et al. 2019). However, there is still limited knowledge on how these mesopelagic fishes move within their isolume to maximize prey encounter rate and reduce predator encounters (Christiansen et al. 2022). For most mesopelagic fishes in the northeast Atlantic, all search for food comes with a risk of predation from piscivorous, visual predators, such as saithe *Pollachius virens*, blue whiting *Micromesistius poutassou* and other gadoids (Giske et al. 1990, Rasmussen & Giske 1994, Bjelland 1995). Different ontogenetic stages of the mesopelagic fish species Mueller's pearlside *Maurolicus muelleri* have been studied extensively in fjord systems. During winter, juvenile and adult pearlside form 2 distinct scattering layers, where juveniles vertically migrate and forage throughout the winter (Giske & Aksnes 1992, Staby et al. 2013, Prihartato et al. 2015), while adults probably trade off predation risk with lower food levels due to their higher visibility to piscivorous predators (Giske & Aksnes 1992). Some types of active predator-avoidance behaviour by mesopelagic fish have been observed, including 3-dimensional (3D) stepwise upwards migration (Kaartvedt et al. 1998, Torgersen & Kaartvedt 2001, Christiansen et al. 2019), and reduced activity during nighttime (Christiansen et al. 2021). There have also been some observations of schooling behaviour (Kaartvedt et al. 1998) and group formation (Benoit-Bird et al. 2017). However, in a 3D environment with no physical structures and natural hiding places, there are likely strong selective pressures on the 3D swimming patterns themselves, especially as food search is accompanied by predation risk. Swimming patterns in planktonic organisms have been shown in the laboratory to emerge by the optimization of prey encounters while reducing predation risks (Bianco et al. 2014). In that study, the search volume self-overlap was used to describe optimal swimming patterns in zooplankton groups, and it showed that different swimming behaviour can produce large changes in encounter rates with predators and prey (Visser & Kiørboe 2006, Bianco et al. 2014). Self-overlap is described by Bianco et al. (2014) as

$$\psi(r) = 1 - \frac{V(r)}{V_{\max}(r)} \quad (1)$$

where ψ expresses how much the clearance volume around the movement trajectory overlaps within itself. It is a function of the actually scanned volume ($V(r)$) and the maximal scanned volume for a given visual range ($V_{\max}(r)$). Values of self-overlap range between 0 and 1, depending on the tortuosity of the trajectory. Ideally for a foraging prey individual, a low degree of self-overlap within its own visual range and a large degree of self-overlap with regards to the predators' visual range would provide relatively higher protection while the search volume is maximal.

In this study, we recorded individual pearlside and glacier lanternfish (*Benthosema glaciale*) abundances and movements in mesopelagic layers in a Norwegian fjord with 5 split-aperture broadband echo sounders. Our hypotheses were that (1) the fishes move strategically to maximize prey and minimize predator encounters, and (2) that the underlying movement behaviours differ between ontogenetic stages. Using *in situ* acoustic measurements of 3D swimming behaviour, we investigated if and how the fishes at different depths and ontogenetic stages were trading prey encounters off against predation risk. We compared 2 scattering layers representing 2 different ontogenetic stages of *M. muelleri.*

2. MATERIALS AND METHODS

2.1. Hydrographic conditions influencing acoustic measurements

The study area is in Sørfjorden (60.43° N, 5.62° E), the southern part of Osterfjorden surrounding the island Osterøy, Norway. The fjord is at its maximum 425 m deep and has a physical threshold of 170 m at the entrance of the fjord (Dale et al. 2019). It is characterized by cold, fresh surface water, which is typical for Western Norwegian fjords in December (Giske et al. 1990). Vertical profiles of temperature, salinity and oxygen were measured from the surface to 210 m depth with a CTD probe (Fig. S1 in the Supplement at

www.int-res.com/articles/suppl/m14424_supp.pdf). Temperature was lowest at the surface (around 5°C), increasing to 11°C at 20 m depth, with a thermocline from 20 to 70 m, where the temperature stabilized at around 8°C down to 210 m. The surface water had low salinity (18 psu), with a rapid increase in salinity down to 30 m (33 psu) followed by a moderate increase down to 210 m (around 35 psu) (Fig. S1).

2.2. Acoustic monitoring and coverage of different sound scattering layers

Individual swimming trajectories of mesopelagic fish were collected during an experimental acoustic survey with the Norwegian RV 'G. O. Sars'. To resolve the biological components of the fjord, acoustic volume scattering strength (Sv, dB re 1 m^{-1}) was measured on 14 and 15 December 2019 with the ship-mounted echo sounders (18, 38, 70, 120, 200 and 333 kHz) (Simmonds & MacLennan 2007), identifying sound scattering layers from a well-known stock of pearlside, glacier lanternfish, zooplankton and pelagic shrimps (Salvanes et al. 1995, Kristoffersen & Salvanes 1998, Bagøien et al. 2001). These sound scattering layers with mesopelagic fish species are found above the 200 m boundary between the epi- and mesopelagic, as the light attenuation in fjordic water creates an ideal isolume at shallower depth than in the open ocean (Staby & Aksnes 2011). The vessel acoustic data identified 2 pronounced sound scattering layers at 70–100 and 150 m down to the bottom, respectively.

2.3. Qualitative check of acoustic data and identifying layers of pearlside

Two scattering layers were identified (hereinafter: SSL1 and SSL2) at 70–100 m and from 120 m and down to the bottom, respectively (Figs. 1 & 2), covering both the meso- and epipelagic layers. To

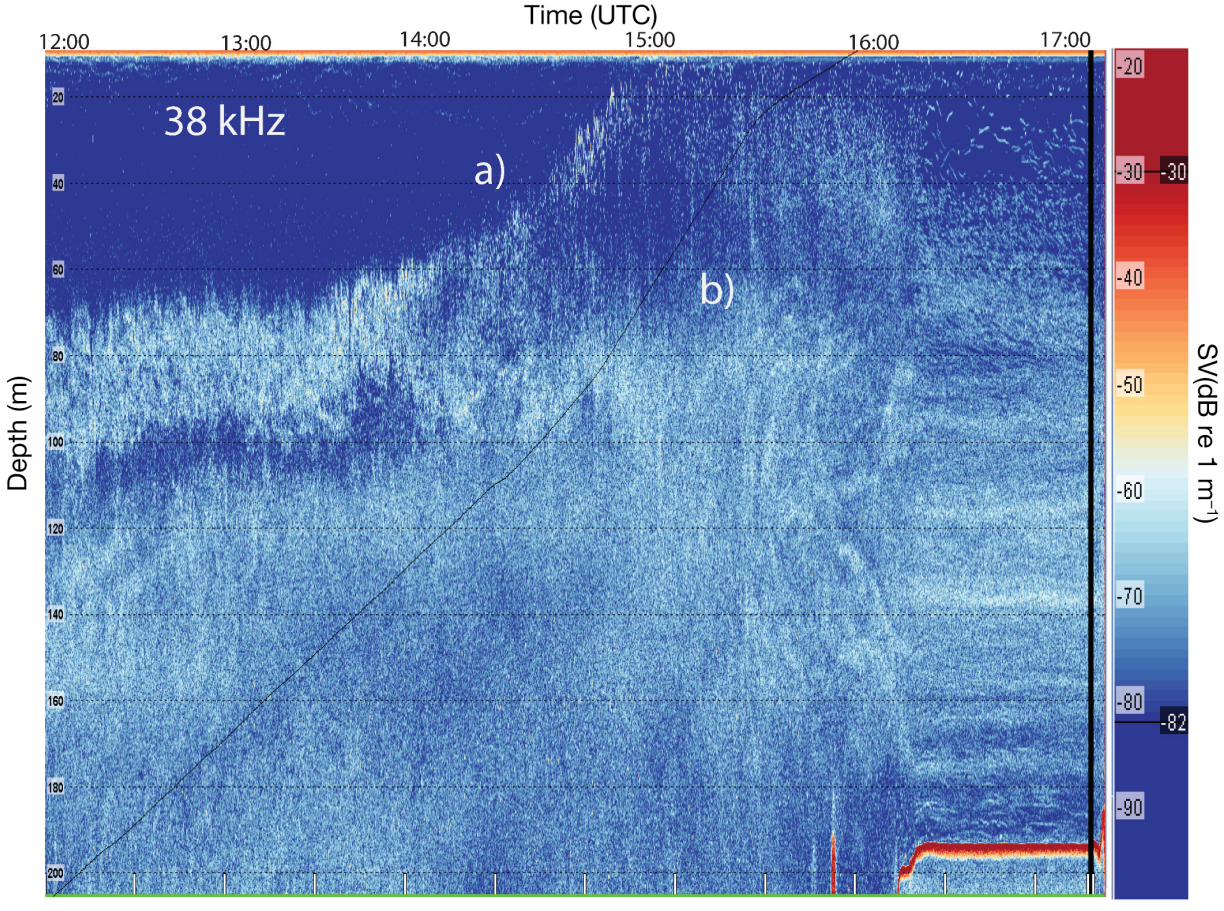

Fig. 1. Ship-recorded echogram displaying volume scattering strength (Sv) of 2 scattering layers: SSL1 (a), consisting of juvenile pearlside migrating towards the surface between ~13:00 and 15:00 h UTC; and SSL2 (b), a mixture of adult pearlside and glacier lanternfish, as well as krill and pelagic shrimps (Table 1)

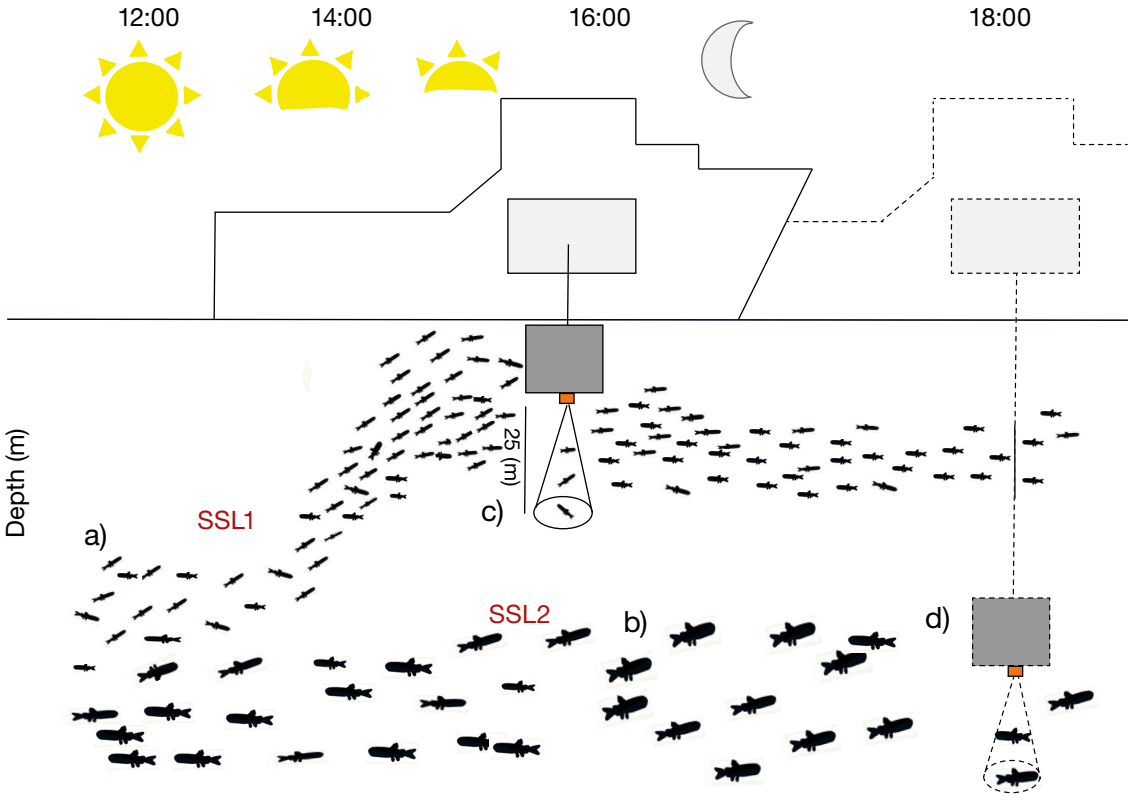

Fig. 2. Experimental design for collecting trajectories and biological samples. The 2 scattering layers (a, SSL1 and b, SSL2) were sampled with the krill trawl at 70 m at 10:00 and 16:27 h UTC. While the ship maintained dynamic position (see Section 2.5), the TS-probe was lowered with a hydraulic winch from the hangar of the ship into the scattering layers SSL1 (c) and SSL2 (d), measuring targets at close range to resolve single targets. The first deployment observed SSL1 during nautical twilight (c). During this period SSL1 had migrated from their daytime depth (70 m) towards the surface to feed and were present at 20–45 m depth. Later the TS-probe was vertically moved down to SSL2 (dashed lines) (d)

ground truth this acoustic profile of the fjord, 2 trawl hauls were performed on 14 December 2019. SSL1 at 70–100 m depth and SSL2 at 150 m depth were towed and covered with a 6 × 6 m 110 µm mesh size macrozooplankton trawl (krill trawl) ('a' and 'b' on Fig. 2). The trawl was towed at a speed of 2.5 and 2.2 m s^{-1} respectively for 10 min (09:09–09:19 and 14:26–14:36 h UTC). The first catch was small and not subsampled. The catch on the second haul was subsampled (species, individual length in mm and mean weight to nearest 0.001 g). The catch was only used as a qualitative check to verify the biological components of the acoustic sound scattering layers.

2.4. Biological components of the fjord system

SSL1 was located at 70–100 m depth during daytime, with the fish forming schools, and migrated towards the surface during dusk ('a' on Fig. 1). The catch composition from the biological sampling with the krill trawl in this layer consisted only of pearlside with mean length (±SD) of 22.3 ± 3.3 mm ('a' on Fig. 1, Table 1). In the daytime, SSL2 extended from around 120 m depth down to the seabed, which was generally deeper than 200 m, and only moved 20 m vertically during the night ('b' on Fig. 1). The fish component of SSL2 consisted of mainly pearlsides with mean length of 29.9 ± 10.4 mm, and adult glacier lanternfish. Other organisms caught in the krill trawl were krill *Meganyctiphanes norvegica* and pelagic shrimps (*Sergestes* spp. and *Pasiphaea* spp.) (Table 1). As described in previous studies (Giske & Aksnes 1992, Prihartato et al. 2015) and also observed in current echograms ('b' on Fig. 1), SSL2 does not migrate. Backscatter from larger fish (target strength [TS] > −40 dB) as observed by the ship-mounted transducers in both SSL1 and SSL2, and with a TS-probe (see Section 2.5) (see 'c' on Fig. 4), was determined to be due to gadoids, i.e. saithe *Pollachius virens* or blue whiting

Table 1. Catch composition from the 2 trawl hauls of the krill trawl with opening angle of 6 × 6 m and 110 µm mesh size. n/a: not applicable

Haul no.	Time (h UTC)	Depth from surface (m)	Towspeed (knots)	Species	N	Individual mean length ± SD (mm)	Catch weight (kg)
1	10:00	70	2.5	*Maurolicus muelleri*	97	22.8 ± 3.33	0.01
2	16:27	152	2.2	*M. muelleri*	3509	29.9 ± 10.4	1.3
2	16:27	152	2.2	*Benthosema glaciale*	1860	34.9 ± 16.78	0.152
2	16:27	152	2.2	*Pasiphaea* spp.	1583	44.9 ± 8.2	0.069
2	16:27	152	2.2	*Sergestes* spp.	8761	37 ± 5.9	0.033
2	16:27	152	2.2	*Meganyctiphanes norvegica*	1455	7.24 ± 1.55	0.450
2	16:27	152	2.2	Mysidae spp.	10	n/a	0.003

Micromesistius poutassou. Identified in a separate study using a multi-net, backscatter properties, target tracking and echocounting, *Calanus finmarchicus*, i.e. the main food source for pearlside, were prevalent in both layers, however with higher density in SSL2 (K. G. Thorvaldsen unpubl. data). SSL1 had fewer recorded tracks of fish compared to SL2 (see 'b' on Fig. 4).

2.5. TS-probe deployment and compiling acoustic data for target tracking

Acoustic single target tracks were collected on December 15 as raw data by Simrad EK80 echosounders (Version 1.12.2.0; EK80 scientific wideband echo sounder, Kongsberg Maritime 2022) with transducers mounted on a lowered acoustic split aperture probe called the TS-probe (Dias Bernardes et al. 2020).

The TS-probe was equipped with 2 broadband transducers with 90–170 kHz and 160–260 kHz acoustic beam field and with an opening angle of 7°. Real-time data were collected using the attached fibre optic cable ('c' and 'd' on Fig. 2). The use of a high ping rate (1–4 Hz) enabled sampling of high-resolution single target tracks. Acoustic data were recorded from 5 to 25 m from the TS-probe beyond the transducer near beam field (Medwin & Clay 1998). The TS-probe hung motionless for several minutes while the vessel was kept in dynamic position (using the vessel's computer system to maintain a fixed position). To assure a low degree of movement of the transducer, pitch and roll were continuously measured simultaneously. The measured tilt and roll were so low that they represented less variation than the inaccuracy of the raw tracking data, with no impact on the final trajectory (Fig. S2). The study area was within a sheltered fjord, and the effect of waves was minimal. The raw echograms were used to confirm that there was no avoidance behaviour from the TS-probe from the observed targets.

The TS-probe was calibrated with a 57.2 mm in diameter tungsten carbide calibration sphere with 6% cobalt binder to obtain reference targets for the 38 kHz narrowband, the 56–87 kHz broadband, and the 97–160 kHz broadband transducers, and a 38.1 mm in diameter tungsten calibration sphere for the 160–260 and 280–450 kHz broadband transducers. The calibrations were performed within International Council for the Exploration of the Sea (ICES) standards (Demer et al. 2015, Ona et al. 2020) (our Table S1).

Trajectories from SSL1 were collected with the 160–260 kHz broadband pulses in the epipelagic from 15:58 to 16:25 h during nautical twilight with respect to the migration that had taken place prior to TS-probe deployment ('c' on Fig. 2). This was done to ensure full overlap between the net sampling and the acoustic data measured by the TS-probe. Trajectories were collected at SSL2 with 90–170 kHz broad band pulses at 120 m total depth from 17:17 to 17:46 h UTC ('d' on Fig. 2) with transducers pointing downwards.

2.6. Identifying and grouping trajectories

Raw acoustic data were post-processed in LSSS (Large Scale Survey System version 2.7.0; Korneliussen et al. 2006), a program used for post-processing of raw acoustic data for biomass estimation, TS measurements and target tracking (Korneliussen & Ona 2002, 2003, Korneliussen et al. 2016). Acoustic scatterers were identified and grouped to mesopelagic fish or smaller plankton groups based on the difference in TS −55 to −75 (dB re 1 m^2) for mesopelagic fish and TS < −75 dB for zooplankton, and the different scattering properties of mesopelagic fish and zooplankton (Martin et al. 1996, Scoulding et al.

2015, Sobradillo et al. 2019), and based on the qualitative check by the krill trawl (Table 1). Swimming trajectories were obtained from both SSL1 and SSL2 during dusk and early night (see Figs. 3 & S3). Single target tracks were initially detected and created in LSSS by using a target tracking algorithm (Handegard et al. 2005, Handegard 2007, Korneliussen 2006), following the same single target echo for an extended period with 4 angular position detections per second.

First, the initial minimum TS (dB) detection threshold for tracked individuals was set to −75 dB to include all sizes of pearlside, as TS is highly variable from ping to ping (Torgersen & Kaartvedt 2001), and TS is usually lower at 200 kHz (Sobradillo et al. 2019) (our Table S2). This could lead to a bias of misinterpreting weaker targets as fish. However, by analysing how TS changes over time for each track during post-processing, the targets with the lowest TS were removed.

The settings made for track initiation were α_0 = 2.8°, β_0 = 2.8°, r_0 = 0.44 m, I_0 = 20 dB. Here, α_0 and β_0 are the maximum along- and athwartship angles within the acoustic beam for initiating a new track, r_0 is the range difference between last terminated track and new initiated track, and I_0 is the minimum difference in TS (dB) for initiating a new track after a previously measured track. The track association settings were basically the same as for track initiation, namely α_G = 2.8°, β_G = 2.8°, r_G = 0.44 (m), I_G = 20 (dB), with α_G and β_G again representing maximum alongship and athwartship cutoff angles, r_G the accepted maximum range between the transducer and 2 following track detections, and I_G is the maximum deviation in TS between 2 subsequent track detections. Setting the range gates high (I_G, r_G) enables the inclusion of fast swimming behaviours, as pearlside are capable of fast bursts of swimming (Christiansen et al. 2021). However, larger range gates also increase the risk of erroneous measurements (Fig. S4). A challenge in choosing long tracks is that it can render a bias towards slow moving organisms. However, upon visual inspection of the tracks in the echogram, most fish tracks were observed to be 60 s or longer (Figs. S2a & S3a). Minimum track length was set to 20 detections. The maximum number of missing detections within a track was set to 8, the number of missing samples was set to 8, and the maximum ratio of missing detections to the total number of detections in a track was initially set to 0.8. However, in the final track dataset, maximum missing detections ratio was never higher than 0.2, increasing the quality of the tracks.

2.7. Detection, initiation and processing of tracks to identify mesopelagic fish trajectories

The aim of this study was to observe mesopelagic fish trajectories, but traditional single echo detection filters used in target tracking often fail in aggregations of fish (Handegard 2007). To increase the number of initially successful trackings, we allowed a lower mean TS than usual in the protocols for TS measurement (Ona 1999). Collecting tracks of multiple fish will lead to errors, and thus tracks were visually inspected in LSSS to manually correct for errors made by the target-tracking algorithm, both by observing the echogram and the anglegram (Fig. S4). We chose tracks with length $t > 60$ s, to secure sufficiently long tracking of varying swimming speed and spatial behaviour. To observe behaviour for as long a time as possible, fragmented tracks due to split errors were manually re-attached in LSSS. In this process, the x (alongship, in m), y (athwartship, in m) and z (vertical distance from transducer, in m) positions of the tracks were exported together with time (UTC) and TS (dB). Erroneous tracks belonging to several individuals were identified due to differences in TS, and large changes in one of the angular positions x, y or z, or radical changes in several of the parameters. The exported x, y and z data from LSSS were further post-processed manually as follows: To reduce the noise in the tracks, erroneous measurements which suggest movements where the measurement of 1 or 2 pings does not follow the remaining trajectory (deviations ± 30 cm per ping), due to an inclusion of another target for 1 or 2 pings in the tracking algorithm, were deleted after visual inspection. To offset the measurement errors commonly made by the phase deviation (Ehrenberg & Torkelson 1996), the curve for all measured points for each ping was smoothed for x, y and z individually, before being reused as the trajectory of the fish. Smoothing was done by fitting x, y and z individually over time t with a piece-wise polynomial smoothing spline in MatLab (MathWorks 2020) with smoothing parameter $p = 0.1$. Since t was unique and equal for x, y and z, predictions for x, y and z at given t could then be merged to 3D trajectories over time. Using these newly computed positions, average and instantaneous swimming speed (W) were calculated by using:

$$W = \sqrt{\left[(x_{t+1} - x_t)^2\right] + \left[(y_{t+1} - y_t)^2\right] + \left[(z_{t+1} - z_t)^2\right]} \quad (2)$$

where x is the alongship angle, y is the athwartship angle and z is the depth, between consecutive points in the trajectories at time t and $t + 1$. The mean swim-

ming speed of the whole trajectory is converted into body length (BL) per second using average BLs of pearlside (Eq. 2) for each scattering layer.

For the self-overlap measurements, we computed the scale-dependent self-overlap, $\psi(r)$ for each trajectory using Eq. (1). The maximum volume is computed as:

$$V_{\max}(r) = \pi r^2 L + -\frac{4}{3}\pi r^3 \quad (3)$$

which considers the trajectory as a straight line, from start to end of the path (L).

Generally, we then have $V(r) \leq V_{\max}(r)$ and depending on the tortuosity of the path, and on the encounter radius, a varying portion of the swept volume is self-overlapping (see Fig. 6A), providing a scale-dependent self-overlap function bounded within 0 and 1, i.e. $0 \leq \psi(r) \leq 1$. In particular, if $\psi(r) = 0$, then the trajectory never intersects itself for that r and the effective volume is equal to the maximum volume; if $\psi(r) = 1$, no new volume is perceived at that r.

Additionally, we expect that when $r \alpha 0$, then $\psi \alpha 0$ and the self-overlap will increase for a larger radius with a maximum at $r < L$. Indeed, at $r \geq L$, $V_{\max}$ and V will both roughly scale as the volume of a sphere taking similar values and providing the limit $r \alpha +^{\circ}$, $\psi \alpha 0$.

A Monte Carlo method can be used to determine the volume of complex or irregularly shaped objects or regions in situations where analytical solutions are not readily available or feasible (Khalos & Whitlock 1988). This method is widely used in various scientific fields, such as physics, engineering and computer graphics, where accurate volume determination is required for simulations, modelling or design purposes (Kroese et al. 2014). In summary, the object of interest is enclosed within a bounding shape, i.e. in our case a cube, then random points are uniformly distributed within the bounding shape. The number of points falling inside the object is compared to the total number of points generated for the cube. The ratio of the volume of the object to the volume of the cube is proportional to the ratio of points falling inside the object to the total number of points. Thus, by multiplying this ratio by the volume of the bounding shape, an estimate of the object's volume can be obtained. The more points generated, the more accurate the volume estimation becomes. However, even with a relatively small number of points, the Monte Carlo method can provide a reasonable approximation, especially for complex or irregular geometries that are challenging to analyse using traditional mathematical approaches (Binder et al. 1993, Bianco et al. 2014).

The Monte Carlo method was used to calculate $V(r)$ (Bianco et al. 2014). We first defined the maximum radius, i.e. the visual range $r_{\max} = 100$ and then for each trajectory computed the bounding box $x_{\min} - r_{\max} < x_{\max} + r_{\max}$ where $x_{\min}$, $x_{\max}$ are respectively the minimum and the maximum value of the trajectory along the x coordinate. Similarly, minimum and maximum values are used for the other coordinates on y and z, and finally the volume of the box V_{box} is calculated. We then drew NP (no. of points) = 2×10^9 random points uniformly distributed within the bounding box, yielding around 1260 points on the vertical and horizontal axes of the cube, and at an edge length of 2 m ca. 2 mm distance between adjacent points. Then we calculated the histogram of the number of points, i.e. $n(r)$ falling at a distance less than a given radius r from the trajectories with the minimum radius at $r_{\min} = 1$ cm, and $r_{\min} \leq r < r_{\max}$. The distance is measured using the interpolating segment between 2 consecutive points on the trajectory. Finally, the effective volume is obtained as:

$$V(r) = \frac{n(r)}{NP} V_{\text{box}} \quad (4)$$

When applying the method to the dataset, we checked that the trajectories were long enough, so that the results are stationary and not influenced by the behaviour at the endpoints.

3. RESULTS

3.1. Classifying individual 3D trajectories and movement patterns

The trajectories displayed a range of different behaviours, from ballistic straight lines to convoluted tracks with high self-overlap (Fig. 3). Some fish were actively ascending or descending with small bursts adjusting their vertical positions (Figs. 4 & 5A). There were also tracks that appeared as long spirals with low self-overlap for a large range of reactive distances (Fig. 3A). This behaviour was observed both in the SSL1 and SSL2 layers. In both layers, there were trajectories with low TS (<–90 dB) with unique movement patterns identified to be *Calanus finmarchicus* (K. G. Thorvaldsen unpubl. data). These targets were ascending and descending with ±20 cm up and down with sharp turns ('b' on Fig. 4). In both samples, traces of larger fish were observed ('c' on Fig. 4). Due to differences in fish density (Fig. S3a), only 10 tracks with sufficient resolution and length >60 s were observed within SSL1, compared to 22 in SSL2. The track lengths ranged from 60 to 490 s.

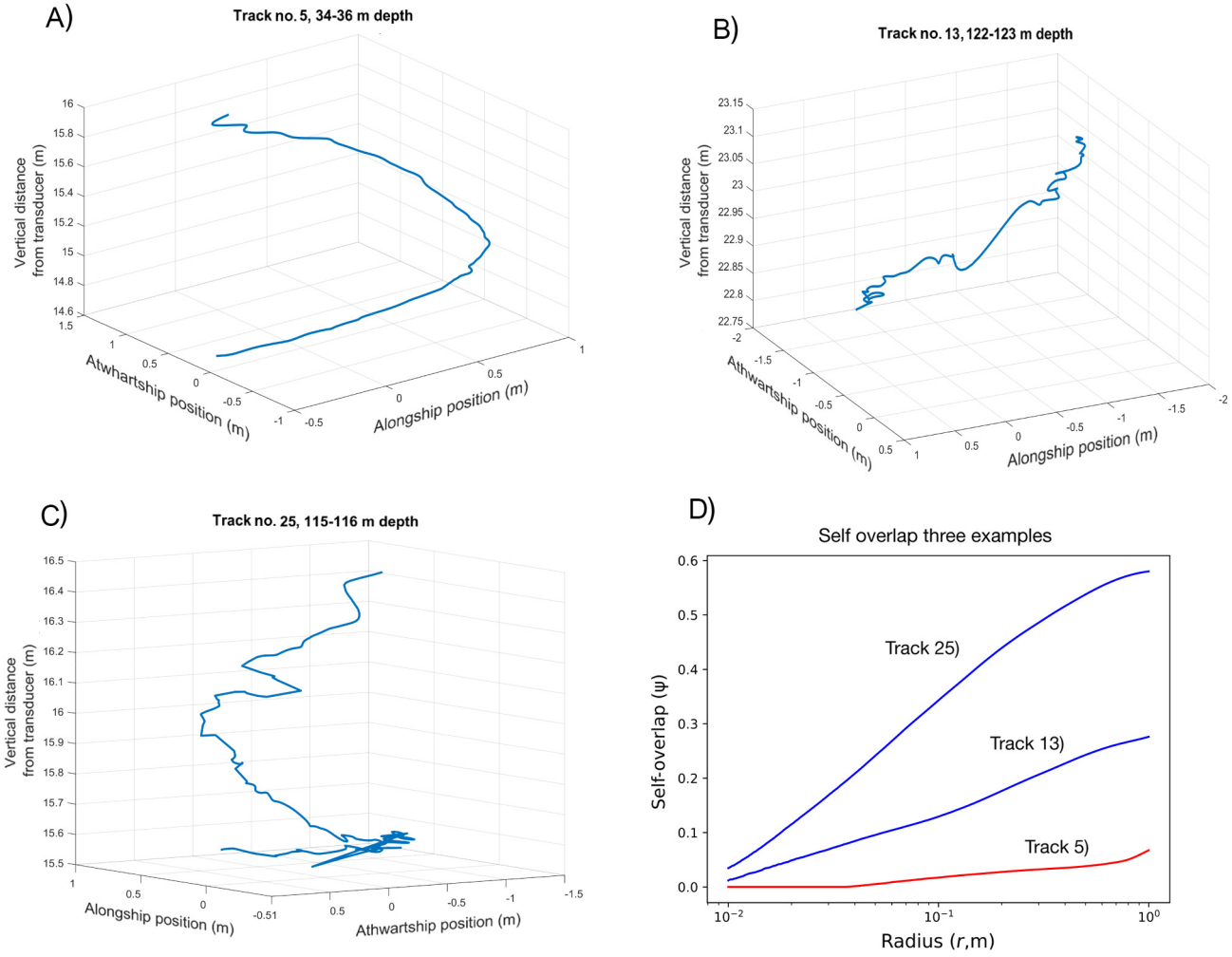

Fig. 3. Three examples of tracks of mesopelagic fish, from (A) SSL1 and (B,C) SSL2, showing the trajectories of the fish in 3D. (D) The measured self-overlap of the 3 tracks where self-overlap ($\psi(r)$) is modelled for several visual ranges

3.2. Swimming speed measurements of individual and groups of accepted fish tracks

The calculated instantaneous swimming speeds (Eq. 2) ranged between 0.01 and 9 BL s^{-1} in SSL1, and 0.1 to 6 BL s^{-1}in SSL2 (Fig. 5). The swimming speeds compared to BL were higher in SSL1 (Fig. 5B). Most swimming speeds were measured to be less than 2 BL s^{-1} (Fig. 5B); the average swimming speed in SSL1 was 0.984 ± 0.55 BL s^{-1}, while in SSL2 it was 0.73 ± 0.42 BL s^{-1}. The instantaneous swimming speeds observed along the tracks were more variable, with some individuals moving with a roughly constant speed while others showed variations in swimming speeds (Fig. 5A). In some cases, the fishes generated bursts of high speed followed by subsequent slower movements (Fig. 3B). In both cases, the average speed (Fig. 5B), as well as the irregularity of some the individual movements (Fig. 5A), suggest active swimming, as both swimming speeds are too fast and patterns too complex to represent passive drifting.

3.3. Analysis of self-overlap measurements for all accepted trajectories

The self-overlap (ψ) measured for the 32 tracks showed values between ψ = 0 and ψ = 0.6 along the range of perception distances from r = 1 cm to r = 100 cm. This range of r is used here to describe typical encounter radiuses for preys and predators. All the tracks show a low degree of self-overlap at the small encounter radius scale (r = 1 cm) and increasing values at higher distances. Hence, tracked individuals had mainly ballistic encounters with their prey,

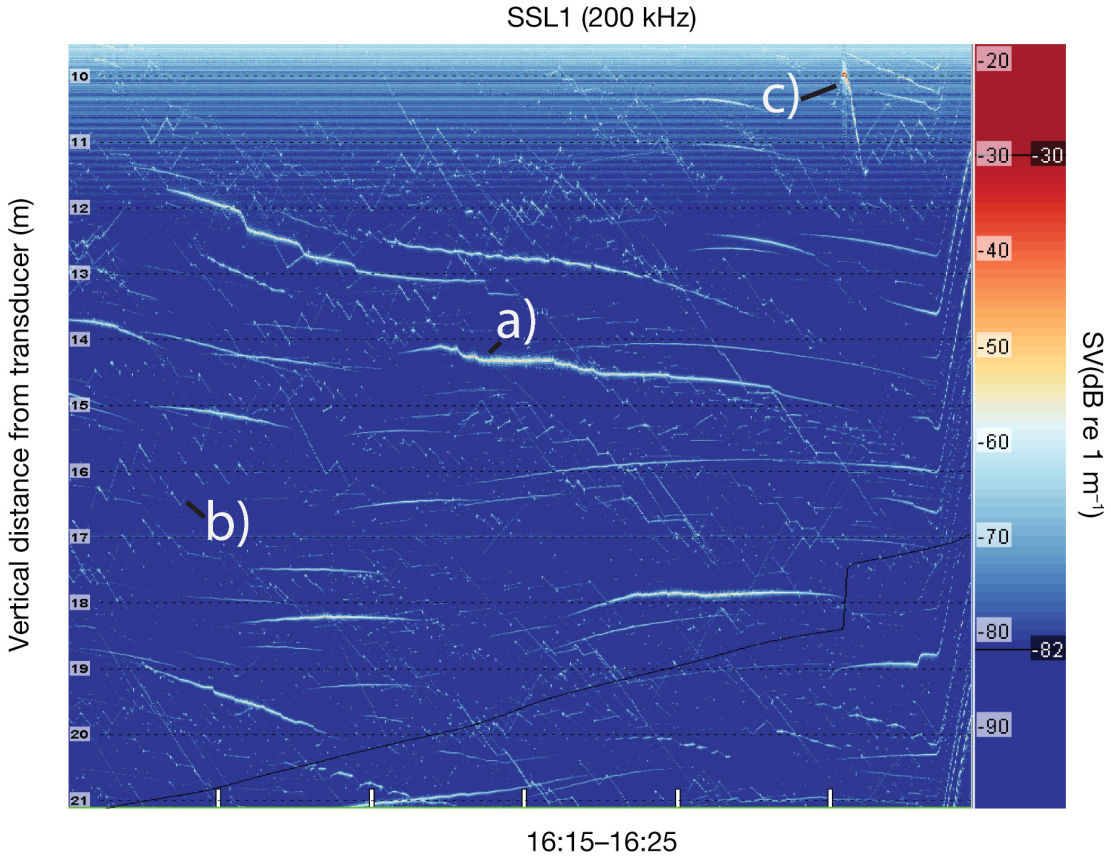

Fig. 4. Echogram of SSL1 volume scattering strength (Sv) recorded with TS-probe between 16:15 and 16:25 h UTC, where single target tracks are visible (a, b and c). Traces from mesopelagic fish (a), zooplankton identified to be *Calanus finmarchicus* (b), and larger predatory fish (c) are present

with values of ψ between 0 and 0.3 for encounter radius between 1 and 5 cm, respectively. In some cases, ballistic encounters were present at both small and large distances. For example, for a few tracks, values of self-overlap never exceeded ψ = 0.1 (Fig. 6A), hence indicating swimming behaviours maximizing volume scanning at all scales. On the other hand, more convoluted trajectories had values close to ψ = 0.6 at r = 100 cm (Fig. 6A), indicating a substantial reduction of volume scanning at larger scales. When grouped together, pronounced differences in self-overlap were evident between the 2 different sound scattering layers (SSL1 and SSL2) (Fig. 6). The average (±SD) self-overlap in SSL1 was lower, with ψ = 0.005 ± 0.02, ψ = 0.13 ± 0.08 and ψ = 0.19 ± 0.09 at 1, 10 and 100 cm, respectively (Fig. 6B). In SSL2, the self-overlap had a mean value of ψ = 0.008 ± 0.03, ψ = 0.17 ± 0.14 and ψ = 0.27 ± 0.19 at 0.01, 0.1 and 1 cm (Fig. 6B), and had a higher average and higher SD than the SSL1. At visual ranges for prey and predators used in this self-overlap model, no individuals performed full self-overlap (ψ = 1).

4. DISCUSSION

We observed a large spectrum of active swimming behaviours for pearlside individuals, and identified differences between juveniles and adults (Fig. 6B). All tracks recorded showed very low values of self-overlap at characteristic scales for prey encounters for small mesopelagic fish (<5 cm). A couple of individual tracks in SSL1 had larger values of self-overlap in the visual range of piscivorous fish, allowing them to reduce encounters with predators in the absence of natural hideouts in the mesopelagic environment. However, these self-overlap values were never higher than 0.3 (Fig. 6B). These tracks generally had a more convoluted movement behaviour, ensuring that the fish can forage new volumes within its own visual range, while the movement appears to be convoluted within the visual range of a larger piscivorous predator (e.g. saithe, blue whiting and haddock) (Giske et al. 1990). The degree of self-overlap in SSL2 was higher. This coincides with results from a neighbouring fjord, where feeding rate was 25

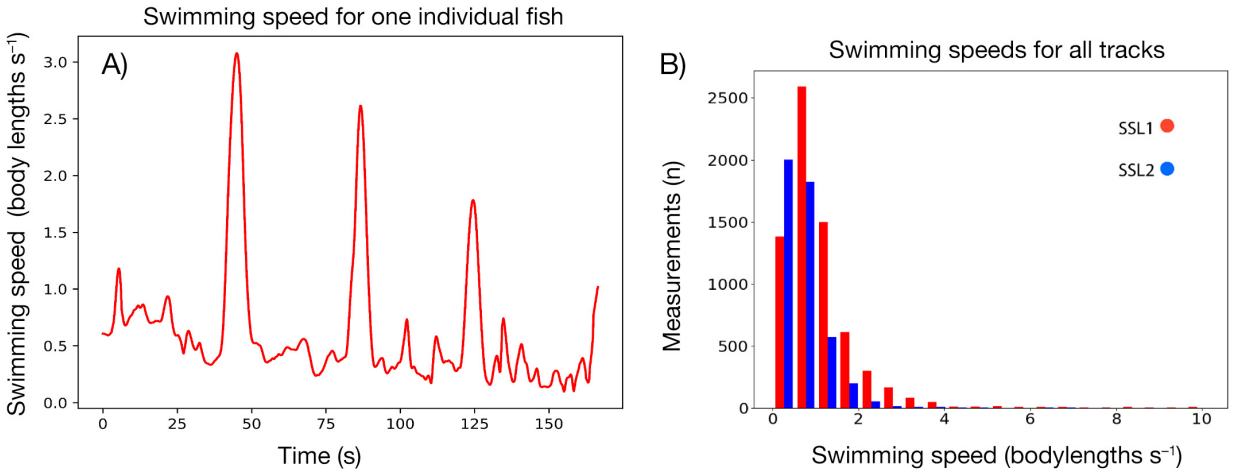

Fig. 5. (A) The short-term swimming speed variability of 1 pearlside from SSL1 for a period of 160 s. (B) Histogram of the frequency of the measured swimming speeds per ping; shown are all measured swimming speeds from SSL1, and from all accepted trajectories for SSL2

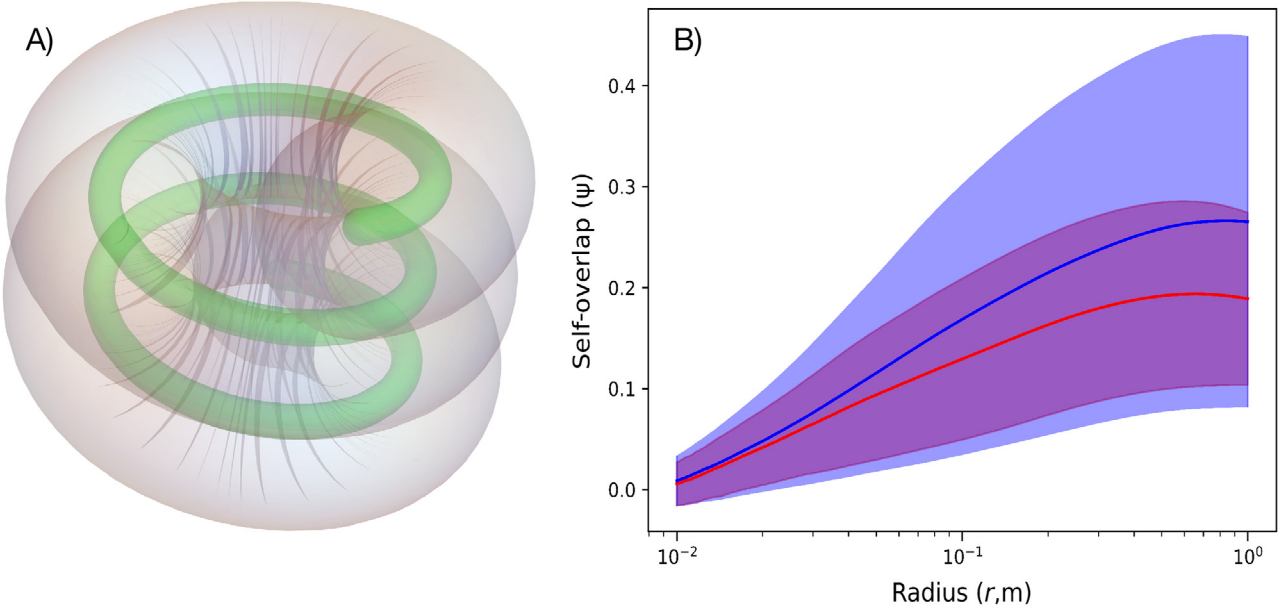

Fig. 6. (A) Illustrative figure for the concept of self-overlap on the perceptive scale of potential predators. On the perceptive scale of mesopelagic fish, the clearance volume (green) is not self-overlapping, i.e. no place is visited twice, and cleared volume per scanned distance is maximal. On the (larger) perceptive scale of a potential predator, potential encounter volume (grey, transparent) where the predator would perceive the mesopelagic fish is highly self-overlapping—hence, the space where the mesopelagic fish might be subject to predation is limited. The trade-off for the mesopelagic fish is, dependent on the spatial distribution of its prey, to minimize self-overlap of its clearance volume while at the same time maximizing self-overlap of the potential encounter volume with predators. (B) The average self-overlap with confidence limits for the trajectories found in the layers SSL1 (red) and SSL2 (blue) with their respective error boundaries as the shaded coloured areas

times lower in this layer compared to SSL1 and mortality was lower (Staby et al. 2013).

Differences in swimming and turning behaviour at dusk have been reported previously (Christiansen et al. 2022). This behaviour can also be found in other oceanic animal groups also living in 3D environments without natural hiding places (Bianco et al. 2014).

The different degrees of self-overlap found in the 32 trajectories most probably reflect a mix of ontogeny, different internal states, different ambient light

conditions influencing visual ranges, micro turbulence and currents, potential mixing with lanternfish as well as different prey and predator densities in vicinity of the observed individuals. There is a predation risk in both SSL1 and SSL2 for pearlside due to the presence of larger fish. However, it is probably heavily reduced in SSL2 due to low ambient light (Staby et al. 2013). The ballistic trajectories observed in SSL1 might represent a bold behaviour, as the search volume is maximal, while self-overlap and hence protection from predation is at a minimum. However, in the more turbid surface water, small juveniles have an advantage compared to piscivorous predators, as the visual range needed to detect copepods is low (Aksnes & Utne 1997, Staby et al. 2013). This will theoretically lead to more encounters with prey, especially if prey are located in patches, which is typical for zooplankton (Folt & Burns 1999), and encounters with predators might be reduced. This behaviour implies that juvenile pearlside are taking higher risks to efficiently ensure somatic growth throughout the winter, as previously reported in Giske & Aksnes (1992). However, juvenile pearlside have lower contrast with the background and can hence afford to migrate higher into the water column where light levels are higher (Giske et al. 1990, Aksnes & Utne 1997, Utne-Palm 2002). Pearlside have previously been described to show different behaviours, where some fishes leave the preferred, safer isolume to forage (Christiansen et al. 2021).

In SSL2, individual behaviours differed more than in SSL1. Low feeding rates and lower natural mortality are prevalent in the deeper layers (Staby et al. 2013), and might explain the higher degree of self-overlap seen in some of the tracks in SSL2, as avoiding predation appears to be the main behaviour of adult pearlside during winter (Giske & Aksnes 1992). Additionally, some of the variability in SSL2 is likely due to a mixing between pearlside and glacier lanternfish. Hence, some of the tracks could belong to lanternfish and can explain the higher variation in the deeper layer, as acoustic and movement pattern discrimination between the 2 species is not easy (Gjøsaeter & Kawaguchi 1980, Gjøsæter 1981, Dypvik et al. 2012, Staby et al. 2013, Scoulding et al. 2015). Finally, internal states would likely play a large role in different behaviours, as the internal state of each trajectory individual is unknown. Hence, it was not to be expected that all measured individuals would show the same behaviour in our study. All trajectories were near *Calanus finmarchicus* individuals based on TS and unique movement patterns and catch data (K. G. Thorvaldsen unpubl. data), which suggests feeding opportunities within visual range. However, even with a lower total amount of zooplankton, the higher light level will result in more encounters between fish and zooplankton in SSL1, which explains why they still vertically migrate (Staby et al. 2013). Many trajectories were showing complex patterns, changing direction frequently within both horizontal and vertical axes or in both directions. During these directional changes, swimming speeds changed. For these cases, we conclude that the fishes are performing active individual search or avoidance behaviour.

The lack of vertical migration of individuals from SSL2 observed by the ship-mounted transducers and catch of only juvenile pearlside in the upper layer indicate that there is limited or no vertical migration by adult pearlside, and supports that the upper layers actually consist of feeding juvenile pearlside. This is supported by previous quantitative and qualitative studies (Giske & Aksnes 1992, Staby et al. 2013, Prihartato et al. 2015). There was also no evidence of vertical migration of the lanternfish below 200 m, even if sporadic migrations have earlier been indicated by trawl catches (Kaartvedt et al. 1988, Rasmussen & Giske 1994, Dypvik et al. 2012).

In this study, a narrow acoustic beam was applied at short range. This was needed to resolve single mesopelagic fishes. However, there is a trade-off between separating single targets and beam width (Ona 1999, Handegard et al. 2005). Targets will eventually move out of the acoustic beam, as the volume of the acoustic beam capable of tracking is usually around 1 m^3, and we acknowledge that behavioural patterns might be shown to vary if we had observed individuals for longer periods. By selecting only high-quality tracks in this study, the number of measurements, especially in SSL1, are low. However, by accepting shorter tracks of lower quality, individual variability would no longer be separable from noise.

With good signal-to-noise ratio and a low density of targets, we believe that the target tracking algorithm is working efficiently. Observing similar and consistent tilt-and-roll angles in SSL1 and SSL2 (Fig. S2), but with different behaviours of fish in the 2 layers, supports our conclusions.

The observed self-overlaps were generally lower than those seen for zooplankton in laboratory studies (Bianco et al. 2014). Tidal currents and/or turbulence might influence the observed movements, especially of zooplankton (Makhlouf Belkahia et al. 2021). However, in our case, most fish trajectories were moving in different horizontal directions across the acoustic beam, and most trajectory shapes were observed to have several directional changes within

the horizontal and vertical planes, as well as significant changes in swimming speed, making it highly unlikely that the observed behaviours are passive and current-driven alone. On the spatio-temporal scales where we observed movements, we assume that predator and prey are dislocated equally by water movements and that hence the relative displacement due to currents is negligible. In future investigations, current speed in the vicinity of tracked individuals could be measured using acoustic-Doppler current profiling, separating swimming behaviour from turbulence and currents.

There are several factors that impact the visual range for both mesopelagic fish and their piscivourous predators, contributing to the individual variations in observed swimming behaviour. The ambient light level was not constant during this study. The TS-probe deployments were conducted during dusk and early night in SSL1, and during night in SSL2, which provides very different ambient light conditions, and thus the perceptive range, i.e. the distance predators are able to detect prey, would vary to a great extent. Pearlsides require mesopic light conditions for successful visual foraging (de Busserolles et al. 2017), which explains why the juveniles migrate to the surface. This is a crucial factor for individual feeding in fish (Aksnes & Utne 1997, Aksnes et al. 2004, Langbehn et al. 2019), which influences both feeding and predation rates and could influence individual movement behaviour accordingly. We assume that the main prey-sensing performed by pearlsides is visual, as tactile predators are dominating in fjords with lower visibility, exemplified in the neighbouring fjord Lurefjorden (Eiane et al. 1999). The visual ranges of the predators, both pearlside and piscivorous fish, rely on the ability to distinguish the silhouette of the prey from the background. Turbidity also has a large impact on visual range of fish (Aksnes & Utne 1997). Small, almost transparent fish and zooplankton can largely increase the reaction distance of a visual predator (Aksnes & Utne 1997), and can thus allow a different isolume than the adult fish (Staby et al. 2013). Fishes in the Sternoptychidae family such as pearlside are known for their counter-illumination photophores, which in theory can make the fish almost invisible if the intensity produced by the photophores matches the ambient light levels (Young & Roper 1976, Mensinger & Case 1990).

The observed behaviours, though highly variable, deviate from random movements. Mesopelagic fish apply spatial strategies that modify encounter rates with their prey and predators. Hence, each individual of either predator or prey populations modifies its expectations of random encounters. Predator–prey dynamics consequently do not follow the principle of mass action, as still assumed by many mathematical models for encounter rates (Gerritsen & Strickler 1977, Rothschild & Osborne 1988, Aksnes & Utne 1997, Huse & Fiksen 2010), functional response (Holling 1959, 1966, Gentleman et al. 2003) and population dynamics (Lotka 1920, Volterra 1926, Turchin 2003).

The application of lowered echosounders and acoustic tracking of several biological trophic levels simultaneously *in situ* in 3D provides a means to study animal ecology, encounters and interactions of undisturbed individuals in their natural environment in the sea. Working with trajectories allows for a more precise measurement of *in situ* clearance volumes as well as natural individual behaviour deviating from randomness and probably increasing evolutionary fitness. On this small scale, behaviour is not uniform, but highly depends on several factors that need to be measured *in situ* and understood at the same small spatial and temporal scales to understand their effects on encounters and their scaling to heterogeneous population dynamics mechanistically.

Acknowledgements. We thank the crew of RV 'G. O. Sars' for the help in data collection, and Professor Egil Ona for making sure the TS-probe was collecting data properly. The production of the manuscript was funded by the H2020 PANDORA project grant agreement No. 773713, and by the project H2020-MEESO ('Ecologically and economically sustainable mesopelagic fisheries', grant agreement No. 817669). Special thanks to Nils Olav Handegard for constructive comments and feedback.

LITERATURE CITED

Aksnes DL, Utne ACW (1997) A revised model of visual range in fish. Sarsia 82:137–147

Aksnes DL, Nejstgaard J, Sædberg E, Sørnes T (2004) Optical control of fish and zooplankton populations. Limnol Oceanogr 49:233–238

Alvheim AR, Kjellevold M, Strand E, Sanden M, Wiech M (2020) Mesopelagic species and their potential contribution to food and feed security — a case study from Norway. Foods 9:344

Ashraf I, Godoy-Diana R, Halloy J, Collignon B, Thiria B (2016) Synchronization and collective swimming patterns in fish (*Hemigrammus bleheri*). J R Soc Interface 13:20160734

Bagøien E, Kaartvedt S, Aksnes DL, Eiane K (2001) Vertical distribution and mortality of overwintering *Calanus*. Limnol Oceanogr 46:1494–1510

Barraquand F, Murrell DJ (2013) Scaling up predator-prey dynamics using spatial moment equations. Methods Ecol Evol 4:276–289

Benoit-Bird KJ, Moline MA, Southall BL (2017) Prey in oceanic sound scattering layers organize to get a little help from their friends. Limnol Oceanogr 62:2788–2798

Bianco G, Mariani P, Visser AW, Mazzocchi MG, Pigolotti S (2014) Analysis of self-overlap reveals trade-offs in plankton swimming trajectories. J R Soc Interface 11: 20140164

Binder K, Heermann D, Roelofs L, Mallinckrodt AJ, McKay S (1993) Monte Carlo simulation in statistical physics. Comput Phys 7:156–157

Bjelland (1995) Life-history tactics of two fjord populations of *Maurolicus muelleri*. CandSci thesis, University of Bergen

Burns AL, Schaerf TM, Lizier J, Kawaguchi S and others (2022) Self-organization and information transfer in Antarctic krill swarms. Proc R Soc B 289:20212361

Christiansen S, Titelman J, Kaartvedt S (2019) Nighttime swimming behavior of a mesopelagic fish. Front Mar Sci 6:1–12

Christiansen S, Klevjer TA, Røstad A, Aksnes DL, Kaartvedt S (2021) Flexible behaviour in a mesopelagic fish (*Maurolicus muelleri*). ICES J Mar Sci 78:1623–1635

Christiansen S, Langangen Ø, Titelman J, Vøllestad LA, Kaartvedt S (2022) Three-dimensional swimming behavior and activity of a mesopelagic fish. Limnol Oceanogr 67:2677–2690

Clark CW, Levy DA (1988) Diel vertical migrations by juvenile sockeye salmon and the antipredation window. Am Nat 131:271–289

Dale T, Bahr G, Harendza A, Velvin R, Palerud R, Szczuciński W (2019) Miljøovervåkning i Sørfjorden ved Osterøy, Technical report 7730, NIVA

Davison PC, Checkley DM, Koslow JA, Barlow J (2013) Carbon export mediated by mesopelagic fishes in the northeast Pacific Ocean. Prog Oceanogr 116:14–30

de Busserolles F, Cortesi F, Helvik JV, Davies WIL and others (2017) Pushing the limits of photoreception in twilight conditions: the rod-like cone retina of the deep-sea pearlsides. Sci Adv 3:eaao4709

Demer DA, Berger L, Bernasconi M, Bethke E, Boswell K, Chu D, Domokos R (2015) Calibration of acoustic instruments. ICES Coop Res Rep 133

Dias Bernardes I, Ona E, Gjøsæter H (2020) Study of the Arctic mesopelagic layer with vessel and profiling multifrequency acoustics. Prog Oceanogr 182:102260

Dypvik E, Røstad A, Kaartvedt S (2012) Seasonal variations in vertical migration of glacier lanternfish, *Benthosema glaciale*. Mar Biol 159:1673–1683

Edgington DR, Cline DE, Davis D, Kerkez I, Mariette J (2006) Detecting, tracking and classifying animals in underwater video. OCEANS 2006, Boston, MA, p 1-5

Ehrenberg JE, Torkelson TC (1996) Application of dual-beam and split-beam target tracking in fisheries acoustics. ICES J Mar Sci 53:329–334

Eiane K, Aksnes DL, Bagøien E, Kaartvedt S (1999) Fish or jellies — a question of visibility? Limnol Oceanogr 44: 1352–1357

Folt CL, Burns CW (1999) Biological drivers of zooplankton patchiness. Trends Ecol Evol 14:300–305

Gentleman W, Leising A, Frost B, Strom S, Murray J (2003) Functional responses for zooplankton feeding on multiple resources: a review of assumptions and biological dynamics. Deep Sea Res II 50:2847–2875

Gerritsen J, Strickler JR (1977) Encounter probabilities and community structure in zooplankton: a mathematical model. J Fish Res Board Can 34:73–82

Giske J, Aksnes DL (1992) Ontogeny, season and trade-offs: vertical distribution of the mesopelagic fish *Maurolicus muelleri*. Sarsia 77:253–261

Giske J, Aksnes DL, Baliño BM, Kaartvedt S and others (1990) Vertical distribution and trophic interactions of zooplankton and fish in Masfjorden, Norway. Sarsia 75: 65–81

Gjøsæter J (1981) Life history and ecology of *Maurolicus muelleri* (Gonostomatidae). Fisk Dir Skr (Ser Havunders) 17:109–131

Gjøsaeter J, Kawaguchi K (1980) A review of the world resources of mesopelagic fish. FAO Fish Tech Pap 193: 123–134

Gong L, Hu Z, Zhou X (2022) A real time video object tracking method for fish. In: Proc 2022 6th Int Conf on Machine Learning and Soft Computing. ACM Int Conf Proc Ser. ACM, New York, NY, p 78–84

Grimaldo E, Grimsmo L, Alvarez P, Herrmann B and others (2020) Investigating the potential for a commercial fishery in the Northeast Atlantic utilizing mesopelagic species. ICES J Mar Sci 77:2541–2556

Handegard NO (2007) Observing individual fish behavior in fish aggregations: tracking in dense fish aggregations using a split-beam echosounder. J Acoust Soc Am 122: 177–187

Handegard NO, Patel R, Hjellvik V (2005) Tracking individual fish from a moving platform using a split-beam transducer. J Acoust Soc Am 118:2210–2223

Handegard NO, Boswell KM, Ioannou CC, Leblanc SP, Tjostheim DB, Couzin ID (2012) The dynamics of coordinated group hunting and collective information transfer among schooling prey. Curr Biol 22:1213–1217

Hays GC, Ferreira LC, Sequeira AMM, Meekan MG and others (2016) Key questions in marine megafauna movement ecology. Trends Ecol Evol 31:463–475

Hidaka K, Kawaguchi K, Murakami M, Takahashi M (2001) Downward transport of organic carbon by diel migratory micronekton in the western equatorial Pacific: its quantitative and qualitative importance. Deep Sea Res I 48: 1923–1939

Holling CS (1959) Some characteristics of simple types of predation and parasitism. Can Entomol 91:385–398

Holling CS (1966) The functional response of invertebrate predators to prey density. Mem Entomol Soc Can 98: 5–86

Huse G, Fiksen Ø (2010) Modelling encounter rates and distribution of mobile predators and prey. Prog Oceanogr 84:93–104

Kaartvedt S, Aksnes D, Aadnesen A (1988) Winter distribution of macroplankton and micronekton in Masfjorden, western Norway. Mar Ecol Prog Ser 45:45–55

Kaartvedt S, Knutsen T, Holst JC (1998) Schooling of the vertically migrating mesopelagic fish *Maurolicus muelleri* in light summer nights. Mar Ecol Prog Ser 170:287–290

Kandimalla V, Richard M, Smith F, Quirion J, Torgo L, Whidden C (2022) Automated detection, classification and counting of fish in fish passages with deep learning. Front Mar Sci 8:2049

Khalos MH, Whitlock PA (1988) Monte Carlo methods, Volume I: Basics. John Wiley and Sons, New York, Chichester, Brisbane, Toronto and Singapore 1986, Library of Congress QA298.K35 1986. Ber Bunsengesellschaft Phys Chemie 92:560–560

Klevjer TA, Kaartvedt S (2006) *In situ* target strength and behaviour of northern krill (*Meganyctiphanes norvegica*). ICES J Mar Sci 63:1726–1735

Kongsberg Maritime (2022) EK80 scientific wide-band echo sounder. www.kongsberg.com/no/maritime/products/

ocean-science/ocean-science/ekkolodd-for-fiskeri-forskning/ek80/ (accessed 31 May 2022)
Korneliussen RJ, Ona E (2002) An operational system for processing and visualizing multi-frequency acoustic data. ICES J Mar Sci 59:293–313
Korneliussen RJ, Ona E (2003) Synthetic echograms generated from the relative frequency response. ICES J Mar Sci 60:636–640
Korneliussen RJ, Ona E, Patel R, Godø OR and others (2006) The Large Scale Survey System-LSSS. Proc 29th Scandinavian Symposium on Physical Acoustics, Ustaoset, 29 January – 1 February 2006.
Korneliussen RJ, Heggelund Y, Macaulay GJ, Patel D, Johnsen E, Eliassen IK (2016) Acoustic identification of marine species using a feature library. Methods Oceanogr 17:187–205
Kristoffersen JB, Salvanes AGV (1998) Life history of *Maurolicus muelleri* in fjordic and oceanic environments. J Fish Biol 53:1324–1341
Kroese DP, Brereton T, Taimre T, Botev ZI (2014) Why the Monte Carlo method is so important today. Wiley Interdiscip Rev Comput Stat 6:386–392
Langbehn TJ, Aksnes DL, Kaartvedt S, Fiksen Ø, Jørgensen C (2019) Light comfort zone in a mesopelagic fish emerges from adaptive behaviour along a latitudinal gradient. Mar Ecol Prog Ser 623:161–174
Lotka AJ (1920) Analytical note on certain rhythmic relations in organic systems. Proc Natl Acad Sci USA 6:410–415
Lucas J, Ros A, Gugele S, Dunst J, Geist J, Brinker A (2021) The hunter and the hunted — a 3D analysis of predator-prey interactions between three-spined sticklebacks (*Gasterosteus aculeatus*) and larvae of different prey fishes. PLOS ONE 16:e0256427
Makhlouf Belkahia N, Pagano M, Chevalier C, Devenon JL, Daly Yahia MN (2021) Zooplankton abundance and community structure driven by tidal currents in a Mediterranean coastal lagoon (Boughrara, Tunisia, SW Mediterranean Sea). Estuar Coast Shelf Sci 250:107101
Martin LV, Stanton TK, Wiebe PH, Lynch JF (1996) Acoustic classification of zooplankton. ICES J Mar Sci 53:217–224
Martinez-Garcia R, Fleming CH, Seppelt R, Fagan WF, Calabrese JM (2020) How range residency and long-range perception change encounter rates. J Theor Biol 498: 110267
MathWorks (2020) Curve Fitting Toolbox - MATLAB. https://se.mathworks.com/products/curvefitting.html (accessed 28 July 2022)
Medwin H, Clay CS (1998) Sources and receivers. In: Fundamentals of acoustical oceanography. Academic Press, Boston, p 127–152
Mensinger AF, Case JF (1990) Luminescent properties of deep sea fish. J Exp Mar Biol Ecol 144:1–15
Nathan R (2008) An emerging movement ecology paradigm. Proc Natl Acad Sci USA 105:19050–19051
O'Dwyer JP (2020) Beyond an ecological ideal gas law. Nat Ecol Evol 4:14–15
Ona E (1999) Methodology for target strength measurements (with special reference to in situ techniques for fish and mikro-nekton). ICES Coop Res Rep, 235:28-43
Ona E, Zhang G, Pedersen G, Johnsen E (2020) *In situ* calibration of observatory broadband echosounders. ICES J Mar Sci 77:2954–2959
Paoletti S, Nielsen JR, Sparrevohn CR, Bastardie F, Vastenhoud BMJ (2021) Potential for mesopelagic fishery compared to economy and fisheries dynamics in current large scale Danish pelagic fishery. Front Mar Sci 8:720897
Prihartato PK, Aksnes DL, Kaartvedt S (2015) Seasonal patterns in the nocturnal distributionand behavior of the mesopelagic fish *Maurolicus muelleri* at high latitudes. Mar Ecol Prog Ser 521:189–200
Qian ZM, Chen YQ (2017) Feature point based 3D tracking of multiple fish from multi-view images. PLOS ONE 12: e0180254
Rasmussen OI, Giske J (1994) Life-history parameters and vertical distribution of *Maurolicus muelleri* in Masfjorden in summer. Mar Biol 120:649–664
Rieucau G, Holmin AJ, Castillo JC, Couzin ID, Handegard NO (2016) School level structural and dynamic adjustments to risk promote information transfer and collective evasion in herring. Anim Behav 117:69–78
Rothschild BJ, Osborn TR (1988) Small-scale turbulence and plankton contact rates. J Plankton Res 10:465–474
Saba GK, Burd AB, Dunne JP, Hernández-León S and others (2021) Toward a better understanding of fish-based contribution to ocean carbon flux. Limnol Oceanogr 66: 1639–1664
Salvanes AGV, Aksnes D, Fosså JH, Giske J (1995) Simulated carrying capacities of fish in Norwegian fjords. Fish Oceanogr 4:17–32
Scoulding B, Chu D, Ona E, Fernandes PG (2015) Target strengths of two abundant mesopelagic fish species. J Acoust Soc Am 137:989–1000
Simmonds J, MacLennan D (2007) Fisheries acoustics: theory and practice, 2nd edn. Wiley, Oxford
Sobradillo B, Boyra G, Martinez U, Carrera P, Peña M, Irigoien X (2019) Target strength and swimbladder morphology of Mueller's pearlside (*Maurolicus muelleri*). Sci Rep 9:17311
Staby A, Aksnes DL (2011) Follow the light — diurnal and seasonal variations in vertical distribution of the mesopelagic fish *Maurolicus muelleri.* Mar Ecol Prog Ser 422: 265–273
Staby A, Srisomwong J, Rosland R (2013) Variation in DVM behaviour of juvenile and adult pearlside (*Maurolicus muelleri*) linked to feeding strategies and related predation risk. Fish Oceanogr 22:90–101
Standal D, Grimaldo E (2020) Institutional nuts and bolts for a mesopelagic fishery in Norway. Mar Policy 119:104043
Tomaru T, Murakami H, Niizato T, Nishiyama Y, Sonoda K, Moriyama T, Gunji YP (2016) Information transfer in a swarm of soldier crabs. Artif Life Robot 21:177–180
Torgersen T, Kaartvedt S (2001) *In situ* swimming behaviour of individual mesopelagic fish studied by split-beam echo target tracking. ICES J Mar Sci 58:346–354
Turchin P (2003) Evolution in population dynamics. Nature 424:257–258
Utne-Palm AC (2002) Visual feeding of fish in a turbid environment: physical and behavioural aspects. Mar Freshw Behav Physiol 35:111–128
van der Meer J, Callier M, Fabi G, van Hoof L, Nielsen JR, Raicevich S (2023) The carrying capacity of the seas and oceans for future sustainable food production: current scientific knowledge gaps. Food Energy Secur 12:e464
Visser AW, Kiørboe T (2006) Plankton motility patterns and encounter rates. Oecologia 148:538–546
Volterra V (1926) Fluctuations in the abundance of a species considered mathematically. Nature 118:558–560
Young RE, Roper CFE (1976) Bioluminescent countershading in midwater animals: evidence from living squid. Science 191:1046-1048

Editorial responsibility: Ignacio A. Catalán (Guest Editor), Esplores, Spain
Reviewed by: Ø. Fiksen and 1 anonymous referee

Submitted: March 24, 2023
Accepted: August 25, 2023
Proofs received from author(s): October 28, 2023